Optics Letters

Subcycle mid-infrared coherent transients at 4 MHz repetition rate applicable to light-wave-driven scanning tunneling microscopy

Katsumasa Yoshioka,[1] Ippo Igarashi,[2] Shoji Yoshida,[2] Yusuke Arashida,[1,2] Ikufumi Katayama,[1,3] Jun Takeda,[1,4] and Hidemi Shigekawa[2,*]

[1]Department of Physics, Graduate School of Engineering, Yokohama National University, Yokohama 240-8501, Japan
[2]Faculty of Pure and Applied Sciences, University of Tsukuba, Tsukuba 305-8571, Japan
[3]e-mail: katayama@ynu.ac.jp
[4]e-mail: jun@ynu.ac.jp
*Corresponding author: hidemi@ims.tsukuba.ac.jp

Received 14 August 2019; revised 9 October 2019; accepted 9 October 2019; posted 9 October 2019 (Doc. ID 375431); published 30 October 2019

We produce subcycle mid-infrared (MIR) pulses at a 4 MHz repetition rate via the optical rectification (OR) of sub-10 fs near-infrared pulses delivered by an optical parametric chirped pulse amplifier. The coherent MIR pulses generated in a GaSe crystal under an ultrabroadband phase-matching condition contain only 0.58–0.85 oscillation cycles within the full width at half-maximum of the intensity envelope. The use of OR enables excellent phase stability of 56 mrad over 5.6 h, which is confirmed by field-resolved detection using electro-optic sampling. An electromagnetic simulation using a finite integration technique reveals that the peak field strength can easily exceed 10 V/nm owing to the field enhancement resulting from focusing MIR pulses onto a tunnel junction.

https://doi.org/10.1364/OL.44.005350

The development of ultrashort phase-locked few-cycle pulses has been subject to intensive research over a vast region of the electromagnetic spectrum ranging from terahertz (THz) to ultraviolet [1–11] to reveal novel phenomena in nonlinear light-matter interactions. In recent years, intense mid-infrared (MIR) pulses have attracted significant attention owing to their advantageous characteristics of low photon energy, large ponderomotive energy, and faster field oscillation than those of typical electron scattering in solids. Exploiting these advantages, MIR pulses can induce various exotic quantum phenomena such as Floquet-Bloch and Volkov states in a topological insulator [12], the acceleration and recollision of quasiparticles in a transition metal dichalcogenide [13], high-harmonic generation in a semiconductor [14], and bright attosecond pulses from noble gases in the soft x-ray region [15]. As with THz [16,17] and near-infrared (NIR) [18,19] pulses, the combination of MIR pulses with a nanoplasmonic system will further accelerate the ongoing revolution of light wave electronics [13–19] by exploiting locally enhanced near fields. In particular, the use of a tunnel junction is the most promising means of producing efficacious near fields whose field enhancement factor α is expected to be on the order of λ/d (λ is the incident wavelength, and d is the nanometer-scale gap width) [20].

Recently, light-wave-driven scanning tunneling microscopy (STM) has been realized using carrier-envelope-phase (CEP)-stable THz pulses with a huge field enhancement factor of $\sim 10^5$ [21–26], and electron tunneling was coherently manipulated across a tunnel junction. Although THz-field-driven STM enables ultrafast dynamics to be probed and even controlled with atomic spatial resolution [24,25], the time resolution is limited to the sub-picosecond time scale. The use of CEP-stable MIR pulses will significantly improve the time resolution and, therefore, will enable the filming of various ultrafast processes that are unattainable with THz pulses. MIR near-field-mediated nonlinear light-matter interactions can also be studied with unprecedented spatiotemporal resolution, which will pave the way towards light wave nanoelectronics. To accurately steer electrons with a light wave in the nonperturbative regime, a single-cycle or even subcycle pulse is indispensable; the inversion-symmetry-broken light field within the pulse can be used to precisely manipulate the motion of electrons. With the field enhancement factor of $\alpha \sim 10^3$ expected in the MIR region taken into account, a peak field strength of $\sim$100 kV/cm is required to steer electrons in MIR-field-driven STM. Although a single-cycle CEP-stable MIR pulse can be generated by the optical rectification (OR) of broadband few-cycle NIR pulses [27], the reported peak field strength is 15 kV/cm, which is limited by the pulse energy of NIR pulses generated using a Ti:sapphire laser system. Intensive effort has been made to generate highly intense single or subcycle MIR pulses by several techniques, such as OR [3], difference frequency generation (DFG) using two optical parametric amplifiers (OPAs) [5], four-wave mixing through filamentation in a gas [6], adiabatic DFG [7], and the multiplexing of the signal and idler pulses from an OPA [8]. However, the repetition rate of these outputs was limited to kHz order. Furthermore, the

long-term CEP stability remains unreliable because of the complexity of the laser systems. Very recently, 1.16 cycle MIR pulses were generated at a 50 MHz repetition rate by the OR of 2 μm NIR pulses delivered by a high-power fiber laser system [28]. Although this technique will provide a scalable system with a peak field of MV/cm order, its complex building blocks may reduce the stability and usability of the system. Besides, the enhanced asymmetry of light waves with fewer oscillation cycles is indispensable for broadening the range of targets in light-wave-driven STM. Therefore, future applications for light-wave-driven STM require a straightforward optical setup having subcycle pulses with significantly increased repetition rates and CEP stability as well as a markedly improved signal-to-noise ratio while maintaining the peak field strength above 100 kV/cm.

Here, we report the generation of CEP-stable subcycle MIR pulses via OR by employing an optical parametric chirped pulse amplifier (OPCPA) that delivers sub-10 fs NIR pulses. The combination of broadband phase matching in a GaSe crystal and the high average output power from the OPCPA enables the generation of 0.58–0.85 cycle, 190 kV/cm peak field MIR pulses at a repetition rate of 4 MHz. Excellent CEP stability over 5.6 h was demonstrated using electro-optic sampling (EOS). Furthermore, we investigated the MIR near field in a tunnel junction by performing a finite integration simulation. The enhanced near field above the 82 V/nm peak field is highly beneficial for driving electron tunneling as well as studying strong-field light-matter interactions at the nanoscale.

A schematic of the experimental setup is illustrated in Fig. 1(a). A custom-built OPCPA system [29] (venteon OPCPA) was employed to generate subcycle MIR pulses. The repetition rate of the system can be tuned from 200 kHz to 4 MHz by varying the built-in pulse picking and amplifier settings. In the case of a repetition rate of 4 MHz, the maximum output power was 4.3 W. The spectrum of the NIR laser pulse ranged from 650 to 1050 nm, as shown in Fig. 1(b). Figure 1(c) shows the measured temporal profile of the NIR pulses using a D-scan module [30] (Sphere Ultrafast Photonics). The pulse duration was determined to be 8.2 fs at the full width at half-maximum (FWHM).

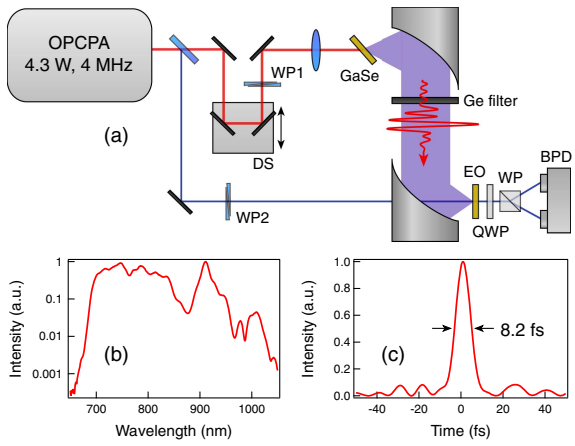

Fig. 1. (a) Generation of subcycle MIR pulses and field-resolved detection using electro-optic sampling. DS, delay stage; WP1 and WP2, wedge plates; EO, electro-optic crystal; QWP, quarter-wave plate; WP, Wollaston prism; and BPD, balanced photodiode. (b) Spectrum of the OPCPA output. (c) Temporal profile of the output NIR pulses obtained by the D-scan method.

The NIR pulses were split into a pump beam and a probe beam for the generation and field-resolved detection of MIR pulses, respectively.

The MIR pulses were generated by OR in a z-cut GaSe crystal [27]. To generate subcycle pulses with ultrabroadband phase matching over the entire bandwidth, we used an extremely thin crystal of 20 μm thickness. The crystal was tilted by an angle of 50° with respect to the direction of the pump beam to satisfy the phase-matching condition. By rotating the emitter crystal around the optic axis, type-I phase matching was selected. The generated MIR pulses were then collimated by a gold-coated off-axis parabolic mirror of 100 mm focal length and refocused by a parabolic mirror of 50 mm focal length onto either a 30-μm-thick GaSe or 450-μm-thick GaP crystal for performing EOS. We also measured MIR pulses using a photoconductive antenna (PCA, BATOP PCA-44-06-10-1030), which simplified the detection setup.

Figure 2(a) shows the MIR electric field transients measured by different detection methods: EOS using a GaSe or GaP crystal and the PCA. Each waveform has a strongly asymmetric shape, which is ideal for accurately steering electrons with a light wave. In the case of the EOS trace measured using a GaSe crystal, the FWHM of the intensity envelope was found to be 31 fs (determined using a Hilbert transform), which corresponds to 0.85 cycles of the carrier wave at a center frequency of 27.5 THz. The Fourier-transformed spectra obtained from the waveforms are shown in Fig. 2(b). The detection scheme using a GaSe crystal highlights the highest-frequency component up to 80 THz (3.7 μm). The low-frequency part below 9.5 THz was not detected owing to the Reststrahlen band of

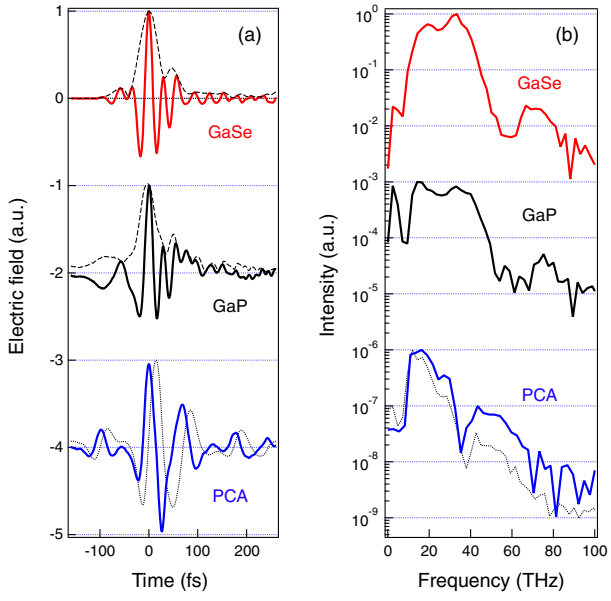

Fig. 2. (a) Field-resolved subcycle MIR pulses detected by different methods: EOS using a 30-μm-thick GaSe crystal with a phase-matching angle of 49°, EOS using a 450-μm-thick GaP crystal, and PCA. The black dashed curve shows the Hilbert transform of the EO trace. The dotted curve shows raw data. For clarity, each waveform is normalized by the maximum peak electric field and offset by 2. (b) Fourier-transformed spectra obtained from the waveforms in (a). The different detection schemes reveal that the generated MIR pulses have an ultrabroadband spectrum spanning the range of 2.4–80 THz (120–3.7 μm).

GaSe [27]. On the other hand, the detection scheme using a GaP crystal is effective for the lowest-frequency component of 2.4 THz (120 μm) with a dip around 8 THz due to the cancellation of the electronic and lattice contributions to the optical nonlinearity [31]. The estimated pulse duration was determined to be 27 fs with 0.58 cycles, which is the shortest among the three traces. From the measured pulse energy of 160 pJ [using a calibrated liquid-nitrogen-cooled mercury cadmium telluride (MCT) detector] and the focal diameter of 100 μm, we obtained a peak electric field strength of 190 kV/cm. To verify the absolute field strength, we also calculated the field strength from the EOS signal of a GaP sensor. By considering the reflection losses and frequency-dependent sensitivity of the detector [3,31], we obtained a peak field of 200 kV/cm, which is in good agreement with that from the energy measurement. In the case of the PCA, we calculated the time derivative of the measured current response to obtain the original electric field [32], and the pulse duration was determined to be 47 fs. The simple optical setup of the PCA might be highly beneficial for measuring MIR pulses inside a vacuum chamber for light-wave-driven STM. Note that the detected waveforms represent the convolution of the actual electric field with the response function of each detection system [31]. Thus, the actual pulse duration could be shorter than 27 fs.

During practical experiments on light-wave-driven STM, measurements with long-term stability over multiple hours are essential. The extremely high stability of our system was therefore demonstrated by measuring MIR waveforms over 5.6 h using EOS without any feedback, as shown in Fig. 3(a). In total, 86 waveforms were taken with a 2 min scan per waveform. Figure 3(b) shows the CEP shift extracted by calculating the instantaneous phase using the Hilbert transform. The standard deviation from its mean value was determined to be 56 mrad over 5.6 h, which is 1-2 orders of magnitude lower than that for OPA-based MIR pulses [9,10]. As can be seen in Fig. 3(c), the first and last waveforms are identical except for the small time drift of less than 2.5 fs. This time drift is most likely due to the timing jitter between MIR and NIR probe pulses, which corresponds to the optical path length of 750 nm. However, to the best of our knowledge, such extreme long-term stability has not been previously demonstrated for single or subcycle MIR pulses.

To develop light-wave-driven STM using subcycle MIR pulses, the estimation of the field enhancement factor α in a tunnel junction is crucial. In the THz spectral range, α was investigated by both experiment and simulation [22,23,25] and was found to be approximately 10^5, which is in good agreement with the value estimated from λ/d [20]. However, despite its importance, no previous studies have focused on the field enhancement of MIR pulses in a tunnel junction. We investigated the MIR near field in a tunnel junction by performing a finite integration simulation (CST MW STUDIO), which shows a quantitative agreement with the experiments in THz-STM [23].

Figure 4(a) shows the tip-sample configuration used in the simulation. The tip was modeled as a cone with a diameter of 0.8 μm and a height of 6.0 μm. The materials used for the tip and sample were tungsten (W) and gold (Au), respectively, which are typically used in STM experiments. A gap width of 1.0 nm and a smallest grid size of 2.5 nm × 2.5 nm × 0.5 nm between the nanotip and the sample were used in the calculation. The actual MIR far-field waveform measured

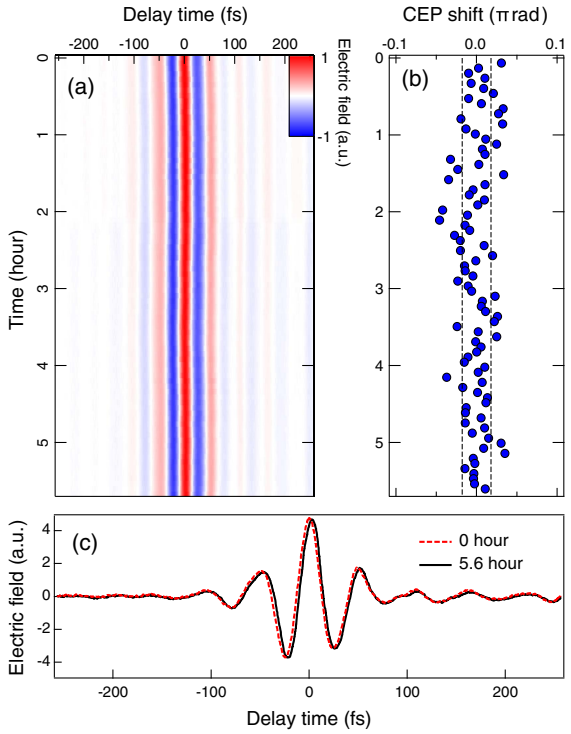

Fig. 3. (a) Long-term stability of the CEP-stable MIR pulses. The MIR waveforms were measured over 5.6 h by EOS using a 30-μm-thick GaSe crystal. (b) Overall CEP shift of MIR waveforms measured over 5.6 h. The black dashed lines indicate the standard deviation of 56 mrad from the mean value. (c) Line plots of the waveforms scanned at $t = 0$ and 5.6 h.

via EOS was incident from a source plane with p polarization and an incident angle of 75°. The time evolution of the MIR electric field was calculated at the midpoint between the nanotip and the sample, as shown in the inset of Fig. 4(b). The calculated α was 4,300, which corresponds to a peak voltage of 82 V in the junction. This α is much higher than that of the isolated resonant tip [33] because of extremely tight confinement. This extremely high electric field is higher than those achieved in the field emission regime [16,17] and sufficient for driving real-space electron tunneling, while the maximum electric field might damage the junction. Note that there is a notable phase shift between the incident far field and the near field. This phase shift might have been due to the antenna effect of the tip [23,26]. In actual experiments, both α and the phase shift differ from tip to tip owing to variations in geometrical shape. Since complete control of the tip shape is very difficult, the *in situ* characterization and manipulation of the MIR near field are highly desirable, similar to those in the case of THz near fields [23,26].

Our system opens new possibilities for light-wave-driven STM with sub-10 fs time resolution. The greatly improved repetition rate and robustness of the system will enable light-wave-driven STM to be combined with additional novel STM methodologies such as scanning tunneling luminescence spectroscopy [34], optical pump–probe STM [35,36], and laser-combined scanning multiprobe spectroscopy [37]. The enhanced MIR near field of 10 V/nm (100 MV/cm) can easily access the nonperturbative regime of condensed matter systems. Furthermore, by tuning the repetition rate of the OPCPA

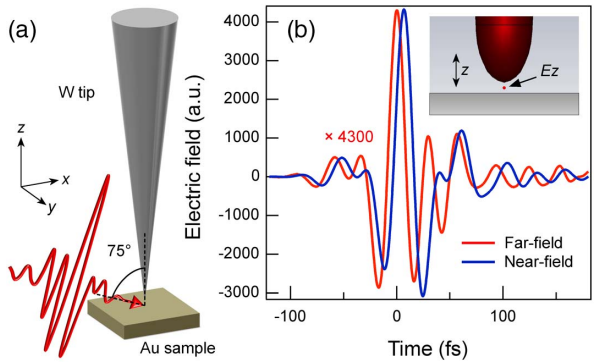

Fig. 4. (a) Tip-sample configuration with a gap width of 1.0 nm. The waveform of far-field MIR electric fields was measured via EOS with a GaSe crystal [Fig. 2(a)]. (b) Far- and near-field waveforms. The electric field is normalized by the peak electric field of the far field. The inset shows a close-up of the tunnel junction.

system to 100 kHz order, the peak field strength reaches the MV/cm range without the use of a nanoplasmonic system, making it capable of ultrafast nonlinear spectroscopy [38] in the subcycle regime.

In summary, by employing a high-power OPCPA system with sub-10 fs NIR pulses, we have successfully generated CEP-stable subcycle MIR pulses at a 4 MHz repetition rate. The field-resolved detection scheme using EOS and a PCA revealed that the subcycle MIR pulses have an ultrabroadband spectrum spanning the range of 2.4–80 THz (120–3.7 μm). The excellent long-term stability of the CEP, the field strength, and the timing jitter between MIR and NIR probe pulses over multiple hours was achieved, which resulted from the robust and straightforward optical setup. From the results of a finite integration simulation, a field enhancement factor of 4,300 was predicted by focusing the MIR pulses onto the tunnel junction of a scanning tunneling microscope. The enhanced MIR near field can greatly improve the temporal resolution of light-wave-driven STM. Because of the ultrabroadband spectrum, high field strength, high stability, and high repetition rate, our system is expected to open the door to strong-field physics as well as ultrafast nanoscale electronics and metrology with an unprecedented signal-to-noise ratio.

Funding. Grants-in-Aid for Scientific Research (17H06088, 16H04001, 18H04288); Japan Society for the Promotion of Science (17J05234); Ministry of Education, Culture, Sports, Science and Technology.

REFERENCES

1. H. Hirori, A. Doi, F. Blanchard, and K. Tanaka, Appl. Phys. Lett. **98**, 091106 (2011).
2. M. Shalaby and C. P. Hauri, Nat. Commun. **6**, 5976 (2015).
3. K. Reimann, R. P. Smith, A. M. Weiner, T. Elsaesser, and M. Woerner, Opt. Lett. **28**, 471 (2003).
4. A. Sell, A. Leitenstorfer, and R. Huber, Opt. Lett. **33**, 2767 (2008).
5. F. Junginger, A. Sell, O. Schubert, B. Mayer, D. Brida, M. Marangoni, G. Cerullo, A. Leitenstorfer, and R. Huber, Opt. Lett. **35**, 2645 (2010).
6. Y. Nomura, H. Shirai, K. Ishii, N. Tsurumachi, A. A. Voronin, A. M. Zheltikov, and T. Fuji, Opt. Express **20**, 24741 (2012).
7. P. Krogen, H. Suchowski, H. Liang, N. Flemens, K. Hong, F. X. Kärtner, and J. Moses, Nat. Photonics **11**, 222 (2017).
8. H. Liang, P. Krogen, Z. Wang, H. Park, T. Kroh, K. Zawilski, P. Schunemann, J. Moses, L. F. DiMauro, F. X. Kärtner, and K.-H. Hong, Nat. Commun. **8**, 141 (2017).
9. K. Kaneshima, N. Ishii, K. Takeuchi, and J. Itatani, Opt. Express **24**, 8660 (2016).
10. M. Knorr, J. Raab, M. Tauer, P. Merkl, D. Peller, E. Wittmann, E. Riedle, C. Lange, and R. Huber, Opt. Lett. **42**, 4367 (2017).
11. A. Wirth, M. T. Hassan, I. Grguras, J. Gagnon, A. Moulet, T. T. Luu, S. Pabst, R. Santra, Z. A. Alahmed, A. M. Azzeer, V. S. Yakovlev, V. Pervak, F. Krausz, and E. Goulielmakis, Science **334**, 195 (2011).
12. F. Mahmood, C.-K. Chan, Z. Alpichshev, D. Gardner, Y. Lee, P. A. Lee, and N. Gedik, Nat. Phys. **12**, 306 (2016).
13. F. Langer, M. Hohenleutner, C. P. Schmid, C. Poellmann, P. Nagler, T. Korn, C. Schüller, M. S. Sherwin, U. Huttner, J. T. Steiner, S. W. Koch, M. Kira, and R. Huber, Nature **533**, 225 (2016).
14. O. Schubert, M. Hohenleutner, F. Langer, B. Urbanek, C. Lange, U. Huttner, D. Golde, T. Meier, M. Kira, S. W. Koch, and R. Huber, Nat. Photonics **8**, 119 (2014).
15. M.-C. Chen, P. Arpin, T. Popmintchev, M. Gerrity, B. Zhang, M. Seaberg, D. Popmintchev, M. M. Murnane, and H. C. Kapteyn, Phys. Rev. Lett. **105**, 173901 (2010).
16. G. Herink, L. Wimmer, and C. Ropers, New J. Phys. **16**, 123005 (2014).
17. S. Li and R. R. Jones, Nat. Commun. **7**, 13405 (2016).
18. M. Krüger, M. Schenk, and P. Hommelhoff, Nature **475**, 78 (2011).
19. T. Rybka, M. Ludwig, M. F. Schmalz, V. Knittel, D. Brida, and A. Leitenstorfer, Nat. Photonics **10**, 667 (2016).
20. K. Yoshida, K. Shibata, and K. Hirakawa, Phys. Rev. Lett. **115**, 138302 (2015).
21. T. L. Cocker, V. Jelic, M. Gupta, S. J. Molesky, J. A. J. Burgess, G. D. L. Reyes, L. V. Titova, Y. Y. Tsui, M. R. Freeman, and F. A. Hegmann, Nat. Photonics **7**, 620 (2013).
22. K. Yoshioka, I. Katayama, Y. Minami, M. Kitajima, S. Yoshida, H. Shigekawa, and J. Takeda, Nat. Photonics **10**, 762 (2016).
23. K. Yoshioka, I. Katayama, Y. Arashida, A. Ban, Y. Kawada, K. Konishi, H. Takahashi, and J. Takeda, Nano Lett. **18**, 5198 (2018).
24. T. L. Cocker, D. Peller, P. Yu, J. Repp, and R. Huber, Nature **539**, 263 (2016).
25. V. Jelic, K. Iwaszczuk, P. H. Nguyen, C. Rathje, G. J. Hornig, H. M. Sharum, J. R. Hoffman, M. R. Freeman, and F. A. Hegmann, Nat. Phys. **13**, 591 (2017).
26. S. Yoshida, H. Hirori, T. Tachizaki, K. Yoshioka, Y. Arashida, Z.-H. Wang, Y. Sanari, O. Takeuchi, Y. Kanemitsu, and H. Shigekawa, ACS Photon. **6**, 1356 (2019).
27. C. Kübler, R. Huber, and A. Leitenstorfer, Semicond. Sci. Technol. **20**, S128 (2005).
28. T. P. Butler, D. Gerz, C. Hofer, J. Xu, C. Gaida, T. Heuermann, M. Gebhardt, L. Vamos, W. Schweinberger, J. A. Gessner, T. Siefke, M. Heusinger, U. Zeitner, A. Apolonski, N. Karpowicz, J. Limpert, F. Krausz, and I. Pupeza, Opt. Lett. **44**, 1730 (2019).
29. O. Prochnow, T. Lang, B. Schulz, J. Ahrens, M. Frede, U. Morgner, and T. Binhammer, Opt. Express **24**, 8074 (2016).
30. F. Silva, M. Miranda, B. Alonso, J. Rauschenberger, V. Pervak, and H. Crespo, Opt. Express **22**, 10181 (2014).
31. A. Leitenstorfer, S. Hunsche, J. Shah, M. C. Nuss, and W. H. Knox, Appl. Phys. Lett. **74**, 1516 (1999).
32. P. U. Jepsen, R. H. Jacobsen, and S. R. Keiding, J. Opt. Soc. Am. B **13**, 2424 (1996).
33. F. Huth, A. Chuvilin, M. Schnell, I. Amenabar, R. Krutokhvostov, S. Lopatin, and R. Hillenbrand, Nano Lett. **13**, 1065 (2013).
34. H. Imada, K. Miwa, M. Imai-Imada, S. Kawahara, K. Kimura, and Y. Kim, Nature **538**, 364 (2016).
35. Y. Terada, S. Yoshida, O. Takeuchi, and H. Shigekawa, Nat. Photonics **4**, 869 (2010).
36. S. Yoshida, Y. Aizawa, Z.-H. Wang, R. Oshima, Y. Mera, E. Matsuyama, H. Oigawa, O. Takeuchi, and H. Shigekawa, Nat. Nanotechnol. **9**, 588 (2014).
37. H. Mogi, Z. Wang, T. Bamba, Y. Takaguchi, T. Endo, S. Yoshida, A. Taninaka, H. Oigawa, Y. Miyata, O. Takeuchi, and H. Shigekawa, Appl. Phys. Express **12**, 045002 (2019).
38. T. Elsaesser, K. Reimann, and M. Woerner, J. Chem. Phys. **142**, 212301 (2015).